Environmental Science and Pollution Research (2024) 31:2732–2744
https://doi.org/10.1007/s11356-023-31104-4

RESEARCH ARTICLE

# Elaboration and characterization of molybdenum titanium tungsto-phosphate towards the decontamination of radioactive liquid waste from $^{137}$Cs and $^{85}$Sr

Ezzat A. Abdel-Galil[1] · Abeer E. Kasem[1] · Sara S. Mahrous[1]

Received: 10 July 2023 / Accepted: 14 November 2023 / Published online: 8 December 2023


## Abstract

The crystalline phase of molybdenum titanium tungsto-phosphate ($MoTiWPO_4$) as an inorganic sorbent material was synthesized via the sol–gel method. The physicochemical characteristics of $MoTiWPO_4$ were evaluated by using Fourier transform infrared (FT-IR), scanning electron microscope (SEM), energy dispersive X-ray (EDX), thermal analysis (TGA-DTA), and X-ray diffraction (XRD). $MoTiWPO_4$ sorbent material exhibits a high chemical resistance to $HNO_3$, HCl, and alkaline media. $MoTiWPO_4$ has good thermal stability as it retained about 75.63% of its saturation capacity upon heating at 500 °C. The sorption studies for several metal ions revealed marked high sorption efficiency of $MoTiWPO_4$ towards $Cs^+$ and $Sr^{2+}$ ions which reached 99% and 95%, respectively. The saturation capacity of $MoTiWPO_4$ for $Cs^+$ and $Sr^{2+}$ is 113 and 109 mg/g, respectively. $MoTiWPO_4$ is approved to be successfully eliminating both $^{137}$Cs and $^{85}$Sr from liquid radioactive waste streams by %eff. of 92.5 and 90.3, respectively, in the presence of competing ions from $^{60}$Co(divalent) and $^{152}$Eu (trivalent), confirming the batch experiment results for the removal of $Cs^+$ and $Sr^{2+}$ metal ions. Furthermore, the decontamination factor exceeds 13.3 in the case of $^{137}$Cs and 10.3 for $^{85}$Sr.

**Keywords** Inorganic sorbents · Cesium · Strontium · Wastewater · Sorption · $MoTiWPO_4$

## Introduction

The operation of nuclear power plants, reprocessing facilities, and research centers, as well as the utilization of radioisotopes in industry and medical diagnostics, all result in the generation of various radioactive wastes. The radioisotopes of strontium and cesium are classified as the most harmful isotopes produced in the nuclear industry due to their long half-life, high chemical activity, migration, toxicity, and relatively small atomic radii (Nasseh et al. 2017; El-Din et al. 2019; Mahrous et al. 2022b).

Developing new or conducting existing treatment methodologies is considered an essential step in nuclear waste safety (Yao et al. 2022). Environmental contamination produced by the periodic discharge of effluents from industrial waste into geo and biospheres has become a global catastrophe, especially in this century. This is owing to the presence of numerous contaminants in these aqueous radioactive and industrial waste streams, which have a severe influence on the health of people and the environment (Feng et al. 2022; Stäger et al. 2023). For example, the spread of these contaminants may reach the groundwater leading to the unstoppable spread of contamination pathways through food and water chains. The contamination spread will produce harmful health effects on humans, animals, and plants. The cancer disease will spread above its normal rate; moreover, the plant and animal growth will be affected making large consequences on the environment (El-Aryan et al. 2014; Yang et al. 2021; Sopapan et al. 2023).

An applicable solution for decreasing the amount of the generated industrial and radioactive waste and treatment

Responsible Editor: Georg Steinhauser

**Highlights**
- Sorbent material based on $MoTiWPO_4$
- $^{137}$Cs and $^{85}$Sr removal form liquid radioactive waste
- Sorption capacity of $^{137}$Cs and $^{85}$Sr
- Kinetic, isotherm and thermodynamics models for $MoTiWPO_4$

✉ Sara S. Mahrous
drsaramahrous.eaea@yahoo.com

[1] Environmental Radioactive Pollution Department, Hot Laboratories and Waste Management Centre, Egyptian Atomic Energy Authority, Cairo, Egypt

methodologies shall take the attention of researchers in the field of radioactive waste management. In the past decades, numerous methodologies have been developed to treat industrial and radioactive liquid waste.

One of the most common treatment processes is solvent extraction used by Patra et al., (2022) for individual extraction of $^{137}Cs$ and $^{90}Sr$ via 1,3-di-octyloxycalix arene-crown-6 (CC6) and dicyclohexano-18-crown-6 [DCH18CH]. Lee et al., (2022) used a flocculation method based on an inorganic washing solution to remove $Cs^+$ and $Sr^{2+}$ from the soil, while co-precipitation was used by Sopapan et al., (2023) via the application of potassium ferrocyanide to remove $^{134,137}Cs$ from low and intermediate level liquid radioactive waste. Also, another advanced technology such as membrane separation, ion exchange, and adsorption has been carried out for the removal of cesium and strontium radionuclides (El-Nagaar et al. 2012; El-Aryan et al. 2014; Rizk and Hamed 2015; Li et al. 2017; Nasseh et al. 2017; Abdel-Galil et al. 2018, 2020, 2021; Mahrous et al. 2019, 2022a, c; Amesh et al. 2020; Pham et al. 2020; Akinhanmi et al. 2020; Bediako et al. 2020; Cheng et al. 2020; Yang et al. 2021; Abass et al. 2022; Lee et al. 2022; Patra et al. 2022; Yao et al. 2022; Șenilă et al. 2023; Sopapan et al. 2023) using organic, inorganic, or composite materials.

Adsorption is widely considered to be the most efficient and practical approach for eliminating metal ions from aqueous solutions. This is due to the improvement of economical adsorbents and adsorbent precursors, as well as their simplicity of handling and operation (Yang et al. 2021). To eliminate metal ions from radioactive and non-radioactive wastewater, several organic and inorganic sorbent materials have been studied. Inorganic materials that are naturally occurring or created synthetically have long been used as adsorbents for different radionuclides, primarily alkali and alkaline earth cations (Abdel-Galil et al. 2018; Bediako et al. 2020; Hai et al. 2020). Due to their strong radiation resistance, thermal and mechanical stability, and compatibility with ultimate waste forms, it is suitable for radioactive waste disposal (Pandiarajan et al. 2018; El-Din et al. 2019; Akinhanmi et al. 2020). Several synthesized inorganic sorbents have significant affinities for one or more radionuclides throughout a broad pH range. These sorbents are adaptable and may be utilized in two different ways, either in granular form in a typical packed-bed installation or in a finely split form in combination with an effective solid–liquid separation method like cross-flow filtering (El-Aryan et al. 2014).

In this study, the preparation of molybdenum titanium tungsto-phosphate sorbent material has been carried out for the selective removal for $^{137}Cs$ and $^{85}Sr$ from liquid radioactive waste streams. The prepared sorbent material is based on the use of inorganic metals such as molybdenum, titanium, tungsten, and phosphate. The saturation capacity, radiation, and thermal stability for $MoTiWPO_4$ sorbent material were investigated. Thermodynamic parameters ($\Delta G^0$, $\Delta S^0$, and $\Delta H^0$) for the adsorption of $Cs^+$, $Sr^{2+}$ onto molybdenum titanium tungsto-phosphate were also calculated. Moreover, the application of $MoTiWPO_4$ in the sorption of $^{137}Cs$ and $^{85}Sr$ from simulated liquid radioactive waste sample in the presence of $^{60}Co$ and $^{152}Eu$ as competing ions was also studied.

## Experimental

Orthophosphoric acid, sodium tungstate, titanium tetrachloride, and ammonium molybdate are made by Sigma-Aldrich and utilized without additional purification.

### Radiotracers

Radiotracers of $^{85}Sr$,$^{60}Co$ and $^{152+154}$ Eu were obtained via the activation reaction ($n$, $\gamma$) by the neutron irradiation of 0.05 g weight of metal chloride salt double wrapped in aluminum foil and transferred via the rabbit system to the vertical irradiation channels inside the core of the second Egyptian Training Research Reactor ETRR-2. $^{137}Cs$ was obtained from a standard radioactive solution purchased from Eckert and Ziegler.

The radioactivity level of the activated samples was measured using coaxial-p type HPGe detector (Canberra, USA) connected to multi-channel analyzer with 16,000 channels (Canberra, USA). The obtained results were analyzed using Gennie 2000 software after energy and efficiency calibration.

### Preparation of chemical reagents

In double-distilled water (DDW), orthophosphoric acid (1.0 M) $H_3PO_4$ and sodium tungstate (0.1 M) $Na_2WO_4{\cdot}2H_2O$ were prepared, while (0.1 M) titanium tetrachloride ($TiCl_4$) was formed in 4.0 M HCl. A solution of 0.1 M ammonium molybdate ($(NH_4)_6Mo_7O_{24}$) (dissolved in deionized water) was prepared; also, 0.1 M $NH_4OH$ to adjust the pH of the solution was diluted.

### Preparation of molybdenum titanium tungsto phosphate ($MoTiWPO_4$)

At $25 \pm 1$ °C, an inorganic precipitate of molybdenum titanium tungsto phosphate was prepared by mixing 250 mL orthophosphoric (1 M) and 250 mL sodium tungstate (0.1 M) solutions with stirring for 30 min to create a homogeneous pale-yellow solution. Then, 250-mL ammonium molybdate (0.1 M) was added to the mixture with stirring for another 30 min. The obtained mixture was then added to 250-mL titanium tetra chloride (0.1 M) with stirring for at least 1 h. Aqueous ammonia was used to alter the pH to 0.9 and stirring until

a green precipitate appeared. The resulting green slurry was left to digest for 24 h at room temperature. After centrifuging the gel, and decanting the supernatant liquid, it was dried at 50 ± 1 °C. The produced precipitate was crushed to get small granules before being converted to $H^+$ form by treating with 1.0 M $HNO_3$ for 24 h with intermittent shaking and replacing the supernatant liquid with new acid. After multiple washes with DDW, the excess acid was removed; the particles were dried at 50 ± 1 °C and sieved to achieve particles of a specific size range (0.12–0.75 mm).

### Characterization of $MoTiWPO_4$

The prepared $MoTiWPO_4$ was examined via several characterization techniques. To examine the surface morphology, scanning electron microscopy, or SEM (JEOL-JSM-6510LA, Tokyo, Japan), was employed. With the use of a Cu-k target and an X-ray diffraction system (Shimadzu XD-D1, Japan), crystal structure, crystalline size, and phase were examined. Using an Oxford Inca EDX detector for compositional analysis, the energy-dispersive X-ray analysis EDX model (JSM-5600 LV, JEOL, Japan) was used for the elemental analysis. A thermogravimetric analysis TGA-DTA test (Shimadzu DTG-60/60H-Thermal Analyzer, Japan) was used to assess the thermal stability. Brunauer, Emmett, and Teller (BET) measurements (Quanta chrome Novawin-Data Acquisition and Reduction for NOVA instruments) were used to obtain the specific surface area, pore volume, and pore size of $MoTiWPO_4$. Last but not least, the active function groups were discovered utilizing FT-IR analysis (FT-IR, Nicolet spectrometer, Meslo, USA.

### Adsorption experiments

Batch tests were performed to determine if the $MoTiWPO_4$ could effectively adsorb $Cs^+$ and $Sr^{2+}$ species from wastewater. The appropriate cation species solution and 50 mg of powdered $MoTiWPO_4$ were used in 15-mL glass bottles for the experiments. For the investigations, a thermostatic shaker with 250 rpm was used to shake the glass containers after they had been sealed; the ambient temperature was set at 298 K. To change the pH, the proper volume of 0.1 M HCl or $NH_4OH$ was applied. Water that has been twice distilled was utilized to make the experiment's solutions. Experiments using solutions with concentrations between 50 and 500 mg $L^{-1}$ to investigate the impact of initial adsorbate concentration were utilized. A contact time of 10 to 300 min is also included. The following formula was used to obtain the removal effectiveness (%R):

$$\%R = \frac{(C_o - C_f)}{C_o} \times 100 \tag{1}$$

The adsorption capacity at any time ($q_t$) and at equilibrium ($q_e$) may be calculated using the following formula:

$$q_e = (C_o - C_{f)} \times \frac{V}{m}\,(\text{mg/g}) \tag{2}$$

and

$$q_t = \left(C_o - C_t\right) \times \frac{V}{m}\,(\text{mg/g}) \tag{3}$$

The decontamination factor (DF) is determined as follows:

$$DF = \frac{A_o}{A_f} \tag{4}$$

### Saturation capacity and thermal effect

Heating the $MoTiWPO_4$ at different drying temperatures (100, 300, 500, and 700 °C) for 4 h in a muffle furnace was used to study the effect of heating on the saturation capacity of the produced sorbent material. Following that, 50 mg of previously heated $MoTiWPO_4$ was placed in a glass container with 5 mL $Cs^+$ ion solution (300 mg/L) at $V/m = 100$ mL/g. For 24 h, the mixture was constantly shaken at 250 rpm in a temperature-controlled incubator shaker (Kottermann D-1362, Germany) until equilibration was achieved. The solution was filtered after achieving equilibrium, and the concentration of $Cs^+$ ions was determined using an atomic absorption spectrophotometer. This process has been done several times with a new $Cs^+$ ion solution or until complete saturation of the prepared $MoTiWPO_4$ with $Cs^+$ ions. The saturation capacity value of $MoTiWPO_4$ (mg/g) was calculated by using the following equation:

$$\text{Capacity (mg/g)} = (C_o - C_f) \times \frac{V}{m} \tag{5}$$

where $C_o$ and $C_f$ represent the concentrations of the ions in solution before and after equilibrium (mg/L), respectively, $V$ is solution volume (L), and $m$ is the mass of the sorbent material(g).

## Results and discussion

### Characterization

#### SEM and EDX

As described in Fig. 1 a, b, and c, the SEM micrographs along with EDX spectrum (d) for the prepared $MoTiWPO_4$ sorbent material. The surface morphology that appears in Fig. 1a demonstrates the microstructure and homogeneity of particle distribution at low magnification powers.

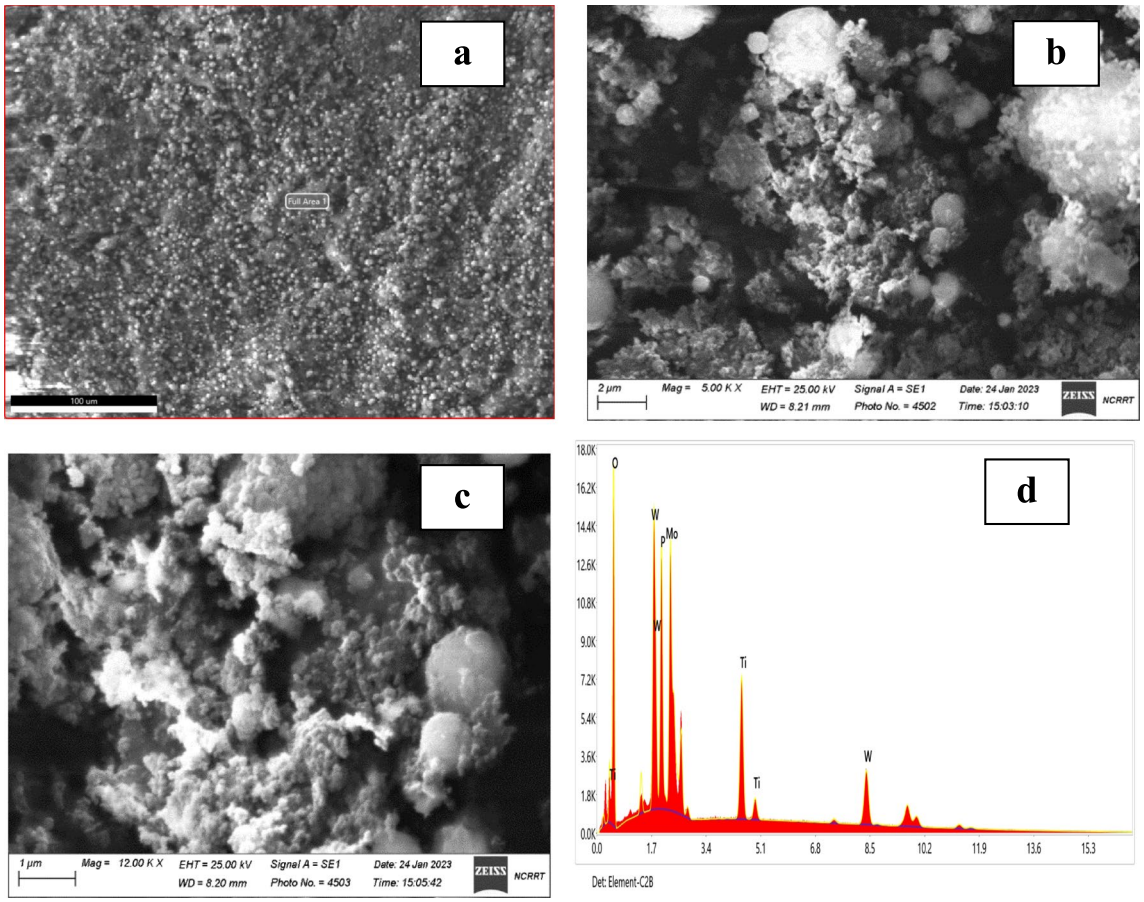


**Fig. 1** SEM and EDX for $MoTiWPO_4$: **a**) the full surface at 100-µm particle size and low magnification power, **b**) × 5000 and **c**) × 12,000; **d**) is the x-ray dispersive energy spectrum from EDX analysis

Figure 2 b and c illustrate the multi-component cavities, gaps, and cracks are created at the inertial distances between the components of the $MoTiWoPO_4$, resulting in the overall high surface heterogeneity, which may be a factor to increase the efficiency of the sorbent material to decontaminate high percent of $^{137}Cs$ and $^{85}Sr$ from liquid radioactive waste. The percentages of the elements for $MoTiWPO_4$ are revealed in Fig. 1d, obtained by the EDX method, and are stated quantitatively in Table 1.

## XRD

Figure 2 shows that $MoTiWPO_4$ has a crystalline nature, which is expected for inorganic materials. Also, the pattern shows many intense peaks at different 2θ value ranges of (10–65°) (Akinhanmi et al. 2020). Using Match (Phase analysis using powder diffraction X-ray) version 3.14 (Germany) software, analysis and matching of the obtained experimental data are conducted. The result of the analysis suggests that the most probable matching occurs with diffraction card no. 96–221-0408 from (crystallography open

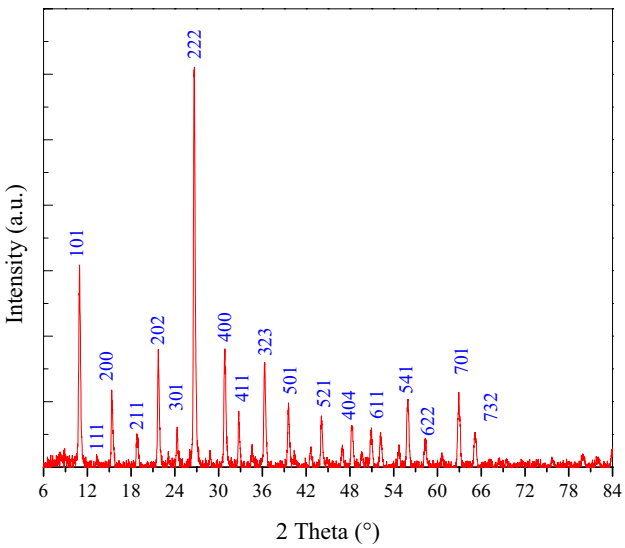


**Fig. 2** XRD pattern for $MoTiWoPO_4$

**Table 1** Elemental composition of $MoTiWPO_4$ sorbent material

| Element | Molybdenum titanium tungsto phosphate | |
|---|---|---|
| | Element (%) | Atomic (%) |
| O | 18.97 | 68.89 |
| p | 11.13 | 8.28 |
| Ti | 8.3 | 4,41 |
| Mo | 30.3 | 5.68 |
| W | 22.9 | 2.75 |

database) COD, given the crystal structure of a cubic with space group Pn-3m (224). The calculated lattice parameter is $a$, $b$, $c = 11.66078$ Å and $\alpha$, $\beta$, $\gamma = 90°$. In addition, the crystalline dimension ($D$, nm) for $MoTiWPO_4$ was calculated using the Bragg angle ($\theta$) and the full width at half maximum (FWHM) by using Debye-Scherer's equation:

$$D = \frac{K\,\lambda}{\beta\,Cos\theta} \tag{6}$$

where $K$ and $\lambda$ are the shape factor (0.9) and the wavelength of Cu–$K_\alpha$ radiation ($\lambda = 0.15406$ nm), respectively. The calculated average crystallite size is 51.62 nm. The degree of crystallinity of the prepared $MoTiWPO_4$ is 97.94%.

### FT-IR

The FT-IR of $MoTiWPO_4$ transmission spectra appears in Fig. 3 and Table 2. Figure 3 (a) shows significant band absorption is about 3420 $cm^{-1}$ equivalent to the stretching vibration of O–H groups of external adsorbed water

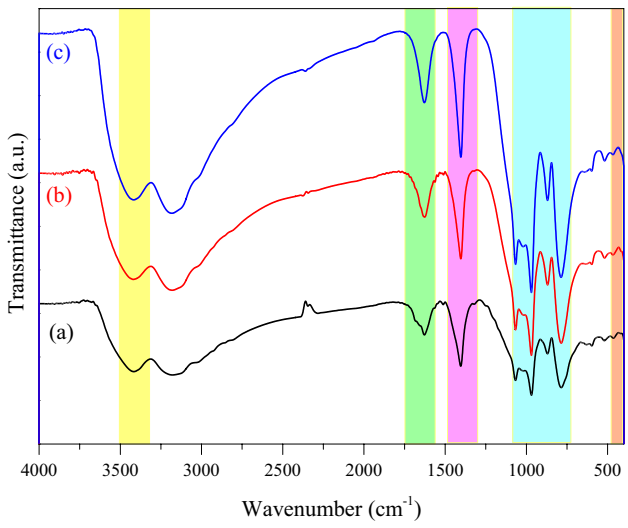


**Fig. 3** FT-IR spectra for $MoTiWPO_4$ sorbent material as a function of wavenumber ($cm^{-1}$) ((a) $MoTiWPO_4$, (b) $MoTiWPO_4$ loaded with $Cs^+$, and (c) $MoTiWPO_4$ loaded with $Sr.^{2+}$)

**Table 2** FT-IR wavenumbers of $MoTiWPO_4$, $MoTiWPO_4/Cs^+$, and $MoTiWPO_4/Sr^{2+}$

| Function group | $MoTiWPO_4$ | $MoTiWPO_4/Cs^+$ | $MoTiWPO_4/Sr^{2+}$ |
|---|---|---|---|
| ν(OH) | 3420 | 3417 | 3417 |
| δ(H2O) | 1626 | 1627 | 1628 |
| $PO4^{3-}$ | 785–1066 | 786–1066 | 787–1066 |
| M–O | —— | 453 | 468 |

(Mahrous et al. 2019). The peak observed at the peak at ≈ 1626$cm^{-1}$ indicates the water molecules' bending mode (El-Aryan et al. 2014). The peak at 1403$cm^{-1}$ corresponds to the metal–OH bond. The phosphate group appears at 785–1066 $cm^{-1}$ (El-Aryan et al. 2014). The IR spectrum of $MoTiWPO_4$ loaded with $Cs^+$ and $Sr^{2+}$ is also given in Fig. 3(b and c) and Table 2. The new peak appears at 453–468 $cm^{-1}$ which can be assigned to metal–oxygen bonds (Mahrous et al. 2022c). From Fig. 3(b and c), a change has been observed in the intensity and wavenumbers of the O–H and phosphate group which may be given to indicate that these functional groups are involved in the sorption process.

### Thermal analysis TGA-DTA

The TGA-DTA profile of $MoTiWPO_4$ is shown in Fig. 4. According to the TGA investigation of $MoTiWPO_4$, there are three different areas where mass is lost up to 700 °C. The initial mass loss owing to humidity is reflected in the first area through heating to 200 °C (Abdel-Galil et al. 2021) where the weight loss is 8.4%. Its corresponding endothermic peak in the DTA curve is observed at 125.07 °C. The second mass loss region observed a weight loss of 6.11% between 200 and 350 °C which may be associated with the condensation of the phosphate group to pyrophosphate groups. Its corresponding endothermic peak in the DTA curve is observed at 250 °C (El-Aryan et al. 2014).

Further weight loss of 3.98% on heating to 490 °C may be due to the elimination of interstitial water molecules from the material (Abdel-Galil et al. 2021). The exothermic peak in the DTA at 500 °C may be due to the structural transformation of the material without weight loss (El-Nagaar et al. 2012).

### Surface area

Surface area is one of the most important characteristics of adsorbents, as the higher its value, the greater the ability of the adsorbent materials to adsorb metal ions from wastewater (Li et al. 2017). For $MoTiWPO_4$, it exhibits an $S_{BET}$ value of ~ 39.5 $m^2/g$, a total pore volume of ~ $3.2 \times 10^{-2}$ cc/g, and an average pore size of ~ 1.6 Å. For comparison with other inorganic sorbent materials, Table 3 lists the

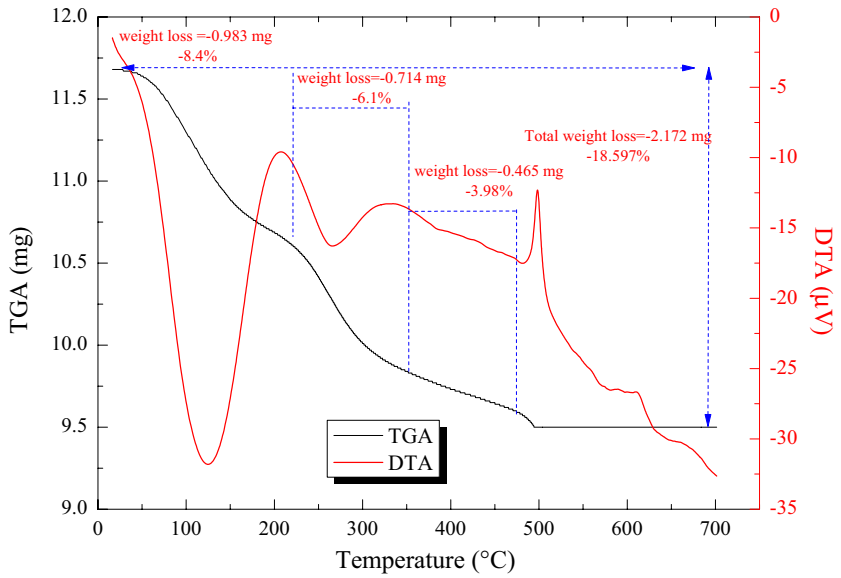


**Fig.4** TGA-DTA for the $MoTiWPO_4$ sorbent material

**Table 3** Comparison between the BET calculation of surface area for different inorganic sorbent materials

| Reference | Material | Surface area ($m^2\ g^{-1}$) | Pore volume ($cm^3\ g^{-1}$) | Pore diameter (nm) |
|---|---|---|---|---|
| Hassan et al. (2019) | Mg/Fe Hydrotalcite | 92.1 | 0.21 | 11.0 |
| Mansy et al. (2017) | $AlSiO_2$/Mg | 0.6 | 4.5E-04 | 14.2 |
| Vasiliev et al. (2019) | Termoxide-39 | 17.0 | — | — |
| Solińska and Bajda (2022) | Clinoptilolite | 28.2 | — | — |
| Solińska and Bajda (2022) | Clinoptilolite / HDTMA-Br | 14.5 | — | — |
| Present work | $MoTiWPO_4$ | 39.5 | 3.2E − 02 | 16.3 |

compared inorganic materials along with the specific surface area computed by the BET method.

Table 3 shows that the present work sorbent material has an intermediate surface area value between the other compared inorganic sorbents. These results enhance its application for the removal of the studied metal ions.

### Point zero charge (PZC)

Point zero charge is the pH value at which the sorbent material's surface has no charges (Abass et al. 2022). The surface of $MoTiWPO_4$ has a positive charge below this pH level to interact with negative species. The negatively charged surface above it interacts with positive species. The $pH_{PZC}$ for $MoTiWPO_4$ is 2.9 as shown in Fig. 5; this value is compatible with the sorption data as will be seen later.

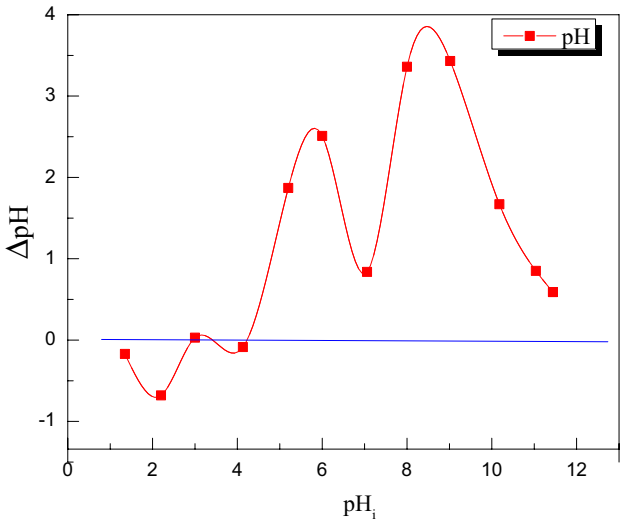


**Fig. 5** Point zero charge for $MoTiWPO_4$

### Chemical dissolution

According to Table 4, the synthesized $MoTiWPO_4$ sorbent material exhibits a high chemical stability in DDW, acids

($HNO_3$ and HCl), and bases (NaOH and KOH). This finding demonstrated that the $MoTiWPO_4$ may be employed in both acidic and basic media, particularly at low concentrations.

## Adsorption batch experiments

### Effect of the adsorbent amount

The impact of adsorbent quantity on the removal of $Cs^+$ and $Sr^{2+}$ was investigated, and the results are given in Fig. 6. The removal of $Cs^+$ and $Sr^{2+}$ behaves similarly, rising with an increase in adsorbent quantity until equilibrium is achieved at the adsorbent quantity greater than 0.05 g as shown in Fig. 6. This pattern can be explained by the fact that when sorbent amounts rise, more active sites become available to adsorb more metal ions until equilibrium is achieved (El-Nagaar et al. 2012; Mansy et al. 2017; El-Din et al. 2019; Hassan et al. 2019; Abdel-Galil et al. 2020; Abass et al. 2022; Mahrous et al. 2022a). As a result, the optimal adsorbent dose for attaining the maximum percent removal is 0.05 g/5 mL.

### Effect of initial concentration

The influence of the adsorbate's initial concentration was investigated by conducting the adsorption experiment with various beginning concentrations of $Cs^+$ and $Sr^{2+}$ (50–500 mg $L^{-1}$) until equilibrium was established; the findings are shown in Fig. 7.

The results reveal that a high percentage of removal was observed at lower concentrations of $Cs^+$ and $Sr^{2+}$ while at high concentrations of cations, the % removal decreased.

**Table 4** The dissolution of $MoTiWPO_4$ in various solvents at 25 ± 1 °C

| Sorbent material | Media | Concentration (M) | Solubility (g/L) |
|---|---|---|---|
| $MoTiWPO_4$ | $H_2O$ | — | B.D |
| | $HNO_3$ | 0.1 | 0.17 |
| | | 0.5 | 0.19 |
| | | 1.0 | 0.20 |
| | | 3.0 | 0.24 |
| | | 5.0 | 0.35 |
| | HCl | 0.1 | 0.19 |
| | | 0.5 | 0.22 |
| | | 1.0 | 0.24 |
| | | 3.0 | 0.28 |
| | | 5.0 | 0.31 |
| | NaOH | 0.1 | 0.28 |
| | | 1.0 | 0.44 |
| | KOH | 0.1 | 0.35 |
| | | 1.0 | 0.43 |

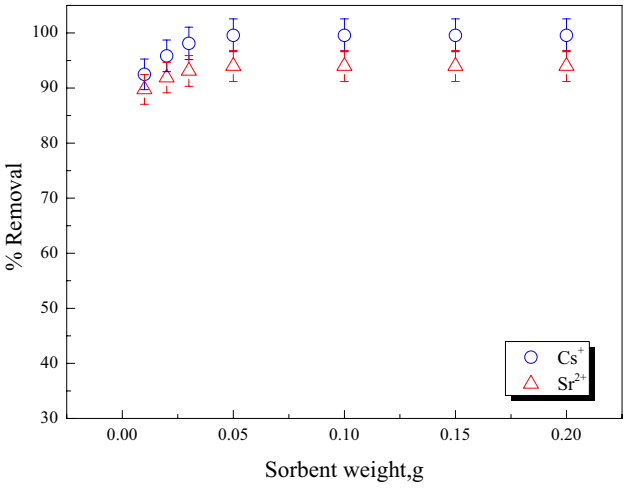


**Fig. 6** The effect of adsorbent amount on $Cs^+$ and $Sr^{2+}$ removal by $MoTiWPO_4$

This result is mostly attributable to the effective adsorbent surface's adsorption site saturation, in which there are accessible unoccupied sites at low concentrations. As the primary $Cs^+$ and $Sr^{2+}$ concentration was raised, the essential active sites for the cations adsorption were rapidly occupied, so the % removal decreased as the concentration increased (Rizk and Hamed 2015).

### Effect of pH

The most significant variable affecting metal ions adsorption onto the adsorbent surface has been identified as aqueous solution pH. This is due to a portion of hydrogen ions themselves competing with adsorbates (Pham et al. 2020). Figure 8 depicts the influence of pH on the removal of $Cs^+$

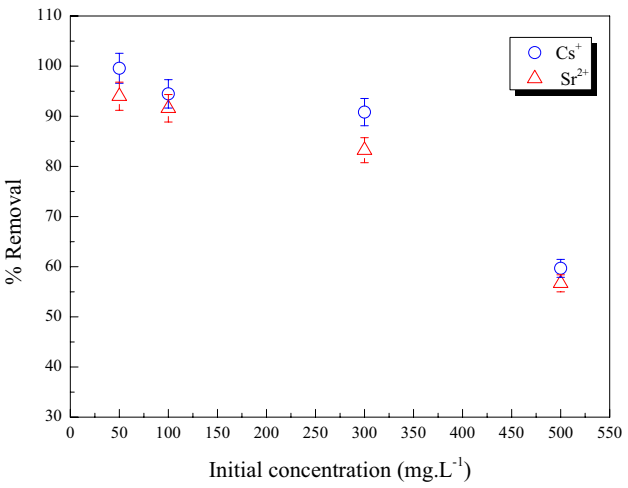


**Fig. 7** The effect of concentration of $Cs^+$ and $Sr^{2+}$ removal by $MoTiWPO_4$

and $Sr^{2+}$ ions from aqueous solutions by $MoTiWPO_4$. It is evident that the $Cs^+$ and $Sr^{2+}$ adsorption efficiency improved quickly with the pH change from 1 to 6. Following that, the rise in adsorption efficiency is gradual until it reaches equilibrium at a pH of 7. So, in order to get the highest adsorption efficiency, a pH of 7 was chosen as the ideal.

### Effect of contact time

Contact time is a major factor in all transfer phenomena, including adsorption. Therefore, it is essential to study how it affects the % removal of $Cs^+$ and $Sr^{2+}$. By carrying out an adsorption test with a starting concentration of 50 mg $L^{-1}$ at various contact durations ranging from 10 to 300 min, the impact of contact time on the adsorption process was investigated. The data shown in Fig. 9 demonstrate that the efficiency of $Cs^+$ and $Sr^{2+}$ adsorption onto the $MoTiWPO_4$ increased with increasing contact time.

The beginning region of the curve showed fast adsorption, which corresponding to the adsorption of the $Cs^+$ and $Sr^{2+}$ on the sites that could be reached quickly on the outside edges of the surface of the sorbent material (Nasseh et al. 2017). When the contact time approached equilibrium, a little decline in adsorption was shown in the second portion of the curve. For all of the examined cations, the equilibrium duration was discovered to be 60 min.

### Effect of temperature

A study of the effects of various temperatures was conducted at 298, 318, 338, and 353 K. The performance of the $MoTiWPO_4$ across the investigated temperature range is shown in Fig. 10. It was evident that the percentage removal increased as the temperature is raised. This would suggest

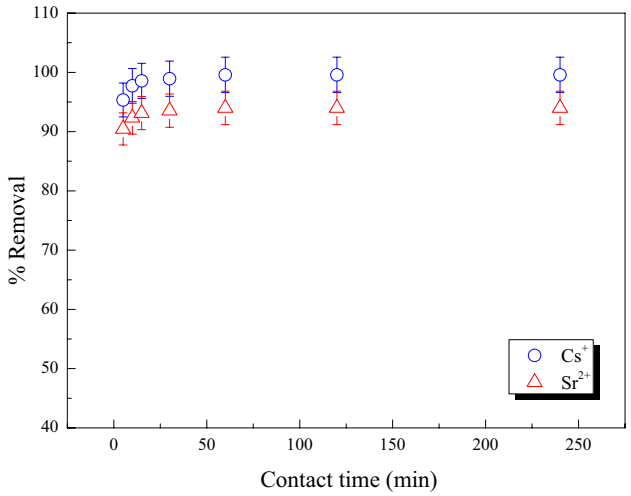


**Fig. 9** The effect of contact time in removing $Cs^+$ and $Sr^{2+}$ by $MoTiWPO_4$

that $Cs^+$ and $Sr^{2+}$ions adsorbed onto $MoTiWPO_4$ has an endothermic character. At an equilibrium duration of 60 min, a rise in temperature from 298 to 353 K causes an increase in the percent removal for $Cs^+$ and $Sr^{2+}$ indicating a temperature-dependent mechanism. This effect may be explained by the availability of additional adsorbent active sites, pore expansion, and/or activation of the adsorbent surface at higher temperatures. This might be owing to the increased mobility of $Cs^+$ and $Sr^{2+}$ ions from the bulk solution to the adsorbent surface, which increased penetration inside $MoTiWPO_4$ (Mahrous et al. 2019; Mansy et al. 2023; Șenilă et al. 2023).

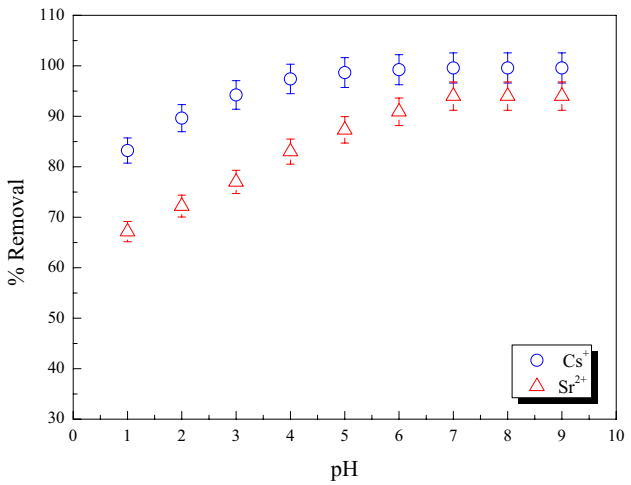


**Fig. 8** The effect of solution pH on removing $Cs^+$ and $Sr^{2+}$ by $MoTiWPO_4$

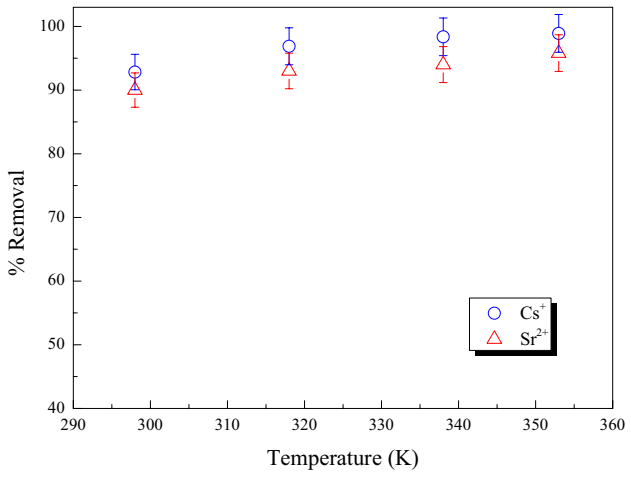


**Fig. 10** The effect of temperature on removing $Cs^+$ and $Sr.^{2+}$ by $MoTiWPO_4$

**Table 5** Effect of temperature on saturation capacity of $MoTiWPO_4$ for $Cs^+$ ions

| Heating temperature (°C) | $Cs^+$ sorption capacity (mg/g) | (%) capacity loss | %Retention |
|---|---|---|---|
| 50 | 113.47 | 0 | 100 |
| 100 | 110.93 | 2.23 | 97.77 |
| 300 | 104.89 | 7.55 | 92.44 |
| 500 | 85.69 | 24.47 | 75.53 |
| 700 | 68.14 | 39.95 | 60.05 |

## Saturation capacity and thermal effect

The saturation capacity of $MoTiWPO_4$ for $Cs^+$ and $Sr^{2+}$ is 113.47 and 109.11 mg/g, respectively. The thermal stability of $MoTiWPO_4$ was studied as a function of saturation capacity for $Cs^+$ ions, and this was achieved by heating the prepared sample at different drying temperature from 50 to 700 ± 1°C, after that, the capacity of $MoTiWPO_4$ for $Cs^+$ ions was determined by batch experiment studies; the data are recorded in Table 5. The data illustrates that the prepared $MoTiWPO_4$ has good thermal stability as it retained about 97.77% of its saturation capacity for $Cs^+$ ions by heating at 100 ± 1 °C, 92.44% by heating at 300 °C ± 1, 75.53% by heating at 500 ± 1 °C, and about 60.05% by heating at 700 ± 1 °C. The saturation capacity of $MoTiWPO_4$ was found to decrease with increasing temperature from 500 to 700 ± 1 °C as observed in Table 5, and this is due to the loss of free and bonded water molecules which may be regarded as the exchangeable active sites (El-Naggar et al. 2014). This behavior is compatible with the obtained results by El-Naggar et al. (2010), El-Naggar et al. (2014), and Tourky et al. (2016).

## Radiation stability

Using a Co-60 gamma-ray irradiator at a dosage rate of 10 kGy/h and absorbed doses of 50, 100, and 150 kGy, the impact of radiation on $MoTiWPO_4$ was studied. The saturation capacity of the material for $Cs^+$ before and after irradiation has been used to assess radiation stability. It was measured and its values are shown in Table 6. It was found that $MoTiWPO_4$ has good radiation stability, losing only around 5.12, 6.4, and 10.61% of its capacity when exposed to radiation at doses of 50, 100, and 150 kGy, respectively (Abdel-Galil et al. 2018). As a result, $MoTiWPO_4$ is thought to be an effective adsorbent for the removal of $^{137}Cs$ and $^{85}Sr$ radionuclides from radioactive waste solution.

## Distribution studies

The distribution coefficient ($K_d$) of $Cs^+$ and $Sr^{2+}$ ions on $MoTiWPO_4$ was calculated using batch equilibration as a function of pH. The values of the distribution coefficient ($K_d$) were assessed using the following equation:

$$K_d = \left[\left(C_i - C_f\right)/C_f\right](V/m) \quad (7)$$

where $C_i$ and $C_f$ are the concentrations of the ions in the solution before and after equilibration, respectively. Plotting the log $K_d$ values vs. the pH of the solutions results in a straight line with a slope ($n$). The findings are shown in Fig. 11 and Table 7, which show how the pH affects the $K_d$ values of the metal ions under study. As shown in Fig. 11 and Table 7, the $K_d$ values of $Cs^+$ and $Sr^{2+}$ ions in the mono-component system increase with the increasing pH of the solution. At low pH, the concentration of hydrogen ions in the solution rises, potentially impeding the mobility of $Cs^+$ and $Sr^{2+}$ ions. In addition, a repulsive interaction was created between the positively charged surface of $MoTiWPO_4$ and

**Table 6** Effect of irradiation doses on the capacity of $MoTiWPO_4$ for $Cs^+$ at a dose rate of 10 kGy/h

| Gamma-ray doses (kGy) | Capacity (mg/g) | Capacity loss (%) | Capacity retention (%) |
|---|---|---|---|
| 0 | 113.47 | 0 | 100 |
| 50 | 108.34 | 5.12 | 94.88 |
| 100 | 107.06 | 6.4 | 93.59 |
| 150 | 102.85 | 10.61 | 89.39 |

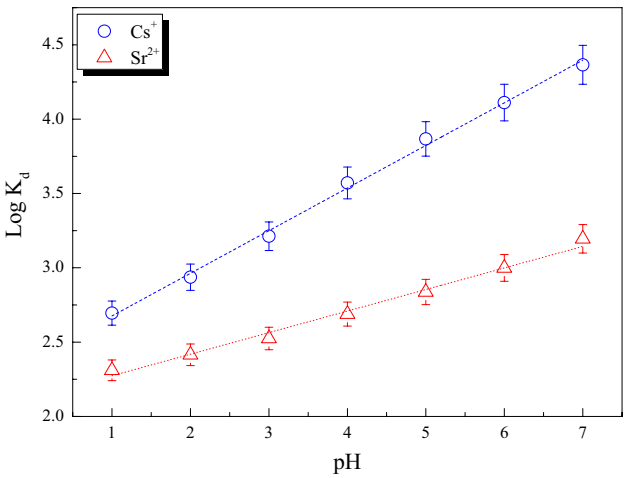


**Fig. 11** Log ($K_d$) as a function of pH for $Cs^+$ and $Sr^{2+}$ on $MoTiWPO_4$

**Table 7** $K_d$ values of $Cs^+$ and $Sr^{2+}$ on $MoTiWPO_4$

| Metal ions | pH of the solutions | $K_d$, mL/g | Ionic radii, Å |
|---|---|---|---|
| $Cs^+$ | 7 | 23,210.25 | 1.67 |
| $Sr^{2+}$ | | 1566.67 | 1.18 |

$Cs^+$ and $Sr^{2+}$ ions in the solution (Abdel-Galil et al. 2018). The sorption of $Cs^+$ and $Sr^{2+}$ ions became more favorable when pH increased due to the presence of an attractive force between the negatively charged surface and these positively charged ions (Abdel-Galil et al. 2018). The best sorption occurs at pH 7, with removal percent and $K_d$ values for $Cs^+$ and $Sr^{2+}$ ions of 99.57% and 23210 mg/L and 94% and 1566 mg/L, respectively. For the ions, $Cs^+$ and $Sr^{2+}$ the slopes of the linear correlations between log $K_d$ and pH are 0.3 and 0.15 respectively. These slopes do not match the valences of the metal ions that have been sorbed, demonstrating the non-ideal ion exchange process.

## Thermodynamic parameters

By examining the distribution coefficient $K_d$ of $Cs^+$ and $Sr^{2+}$ ions sorbed on $MoTiWPO_4$ at various temperatures (298, 318, 338, and 353 K), thermodynamic behavior was investigated. The following equations:

$$\Delta G^o = -RT\ln\left(K_d\right) \tag{8}$$

$$\ln K_d = \frac{\Delta S^o}{R} - \frac{\Delta H^o}{RT} \tag{9}$$

$$\Delta G^o = \Delta H^o - T\Delta S^o \tag{10}$$

were used to compute several thermodynamic parameters, including the standard free energy change ($\Delta G°$, kJ $mol^{-1}$), standard enthalpy change ($\Delta H°$, kJ $mol^{-1}$), and standard entropy change ($\Delta S°$, J $mol^{-1}K^{-1}$) determined from the slope and intercept of the straight line produced by the plot of ln $K_d$ as a function of 1/$T$ (Fig. 12). Table 8 presents the thermodynamic outcomes. The positive value of $\Delta H°$ denotes the endothermic nature of the adsorption process, and the positive value of $\Delta S°$ indicates that the surface randomness increases during the adsorption process. The examined metal ions displayed negative free energy change ($\Delta G°$) values, demonstrating the spontaneity of the adsorption process and the preference of these cations to adsorb on $MoTiWPO_4$. Additionally, the fact that the negativity of $\Delta G°$ rises as the temperature rises suggests that the adsorption process is endothermic and spontaneous (Lagergreen 1907; Olabemiwo et al. 2017).

To compare the present work sorbent material performance with other materials, from the literature review, a comparison for the sorbent materials for different radionuclides is listed in Table 9.

**Table 8** Thermodynamic parameters for sorption of $Cs^+$ and $Sr^{2+}$ by $MoTiWPO_4$

| Ions | Temp. (K) | $\Delta H°$ (kJ $mol^{-1}$) | $\Delta G°$ (kJ $mol^{-1}$) | $\Delta S°$ (J $mol^{-1}$ $K^{-1}$) |
|---|---|---|---|---|
| $Cs^+$ | 298 | 37.86 | −17.09 | 184.4 |
| | 318 | | −21.25 | |
| | 338 | | −24.44 | |
| | 353 | | −26.70 | |
| $Sr^{2+}$ | 298 | 6.45 | −17.46 | 80.25 |
| | 318 | | −19.02 | |
| | 338 | | −20.67 | |
| | 353 | | −22.69 | |

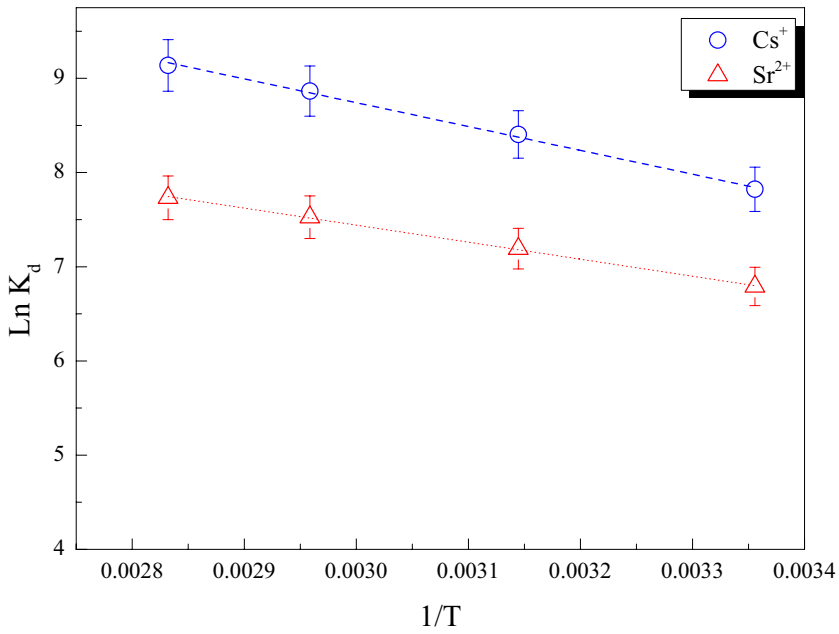


**Fig. 12** Ln ($K_d$) as a function of 1/T for $Cs^+$ and $Sr^{2+}$ on $MoTiWPO_4$

**Table 9** Comparison between sorbent materials for the removal of some radionuclides

| Ref | Sorbent material | pH | Removal efficiency | | | |
|---|---|---|---|---|---|---|
| | | | $^{137}Cs$ | $^{134}Cs$ | $^{90}Sr$ | $^{85}Sr$ |
| Present work | $MoTiWPO_4$ | 7.0 | 92.5 | –– | –– | 90.30 |
| Abdel-Galil et al. (2019) | SnSiMo | 5.0 | 96.5 | –– | 92.70 | –– |
| Ali et al. (2020) | Dowex-HCR resin | 10–11 | –– | –– | –– | 84.0 |
| Attallah et al. (2016) | $PAA/MA/SiO_2/Al_2O_3$ | –– | –– | 77.8 | –– | –– |

## Application

To test the ability of the prepared material ($MoTiWPO_4$) in the efficient removal of the studied radionuclides from low-level liquid radioactive waste sample containing $^{137}Cs$ and adding activated radionuclides such as $^{60}Co$, $^{152}Eu$, and $^{85}Sr$ to simulate the competing ions, radiological experiments were conducted. Before carrying out the application, a radiological characterization of the radioactive waste sample was done using non-destructive gamma-ray spectrometry. The detector was coaxial-P-type HPGe (GEM-series, ORTEC, USA) with efficiency up to 30% and a resolution of 2.0 keV for 1173 and 1330 gamma energies. The detector has been calibrated for energy and efficiency to easily calculate the radioactivity of both cesium and strontium. The radioactivity level of the radioactive waste sample was determined by the following equation given by Hilal et al. (2022) and El Afifi et al. (2023) as

$$A(Bq/L) = \frac{\text{Net Counts-Background}}{t \times \varepsilon \times I_\gamma \times V} \quad (11)$$

In which $A$ is the radioactivity level (Bq/L), $t$ is the counting time, $\varepsilon$ is the detector efficiency, $I_\gamma$ is the probability of emission of each gamma ray, and $V$ is the sample volume in (L). The radiological characterization of the sample reveals that each 10 mL from the sample contains 150 kBq from $^{137}Cs$, 31 kBq $^{60}Co$, 28 kBq $^{152}Eu$, and 74 kBq from $^{85}Sr$. Using a 15 mL-capacity polyethylene vial, mix 1.0 mL from the liquid waste with 9.0 mL distilled water and add 0.1 g from the $MoTiWPO_4$ sorbent material. After that, radiometric counting was carried out to confirm the initial radioactivity level of the sample, then shaking them for 1 h.

After settling by gravity, the decantation process was carried out to find the final radioactivity level of the sample. The result of counting the initial waste sample is plotted in Fig. 13, and the data obtained are listed in Table 10.

It is evident from Table 10 that $MoTiWPO_4$ is proficient in removing both $^{137}Cs$ and $^{85}Sr$ from liquid radioactive waste samples by %eff. of 92.5 and 90.3, respectively, in the presence of competing ions from $^{60}Co$ (divalent) and $^{152}Eu$ (trivalent), confirming the batch experiment results for the removal of $Cs^+$ and $Sr^{2+}$ metal ions. In addition, the decontamination factor reaches 13.3 in the case of $^{137}Cs$ and 10.3 for $^{85}Sr$.

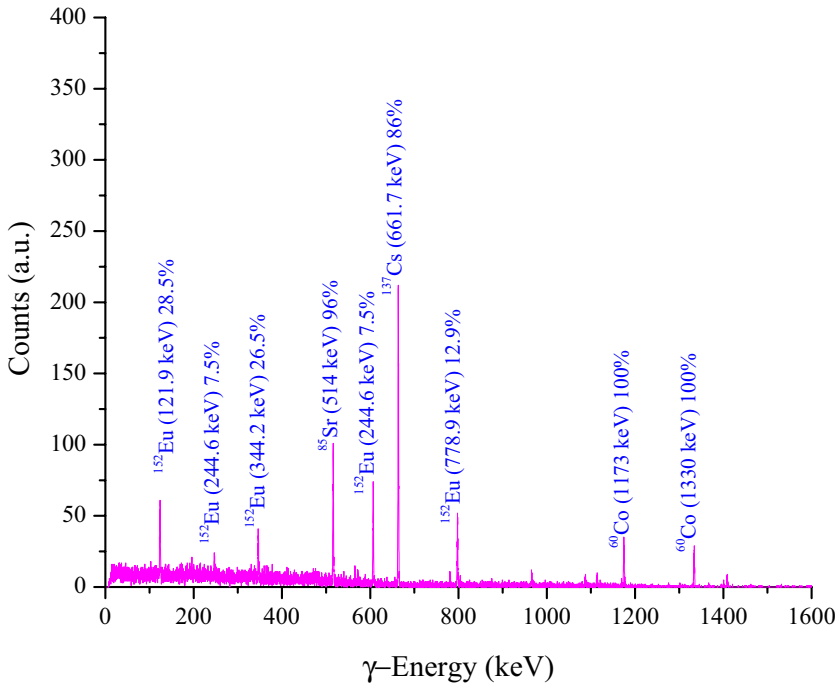


**Fig. 13** Gamma spectra of a radioactive waste characterization measured using HPGe detector giving the gamma energy line along with the probability of emission of each gamma energy

**Table 10** Radioactivity levels of initial and final counting of the waste sample along with the decontamination factor and %eff

| Radionuclides | Initial activity (Bq/mL) | Final activity (Bq/mL) | DF | % eff |
|---|---|---|---|---|
| $^{137}$Cs | 15,000 ± 122.47 | 1125 ± 33.5 | 13.3 | 92.5 |
| $^{85}$Sr | 7,400 ± 86.02 | 717.8 ± 26.7 | 10.3 | 90.3 |
| $^{60}$Co | 3,100 ± 55.57 | 558.0 ± 23.6 | 5.5 | 82.0 |
| $^{152}$Eu | 2,800 ± 52.91 | 1190 ± 34.4 | 2.4 | 57.5 |

## Conclusion

$MoTiWPO_4$ showed promising results in removing $Cs^+$ and $Sr^{2+}$ metal ions from wastewater. It also showed that $MoTiWPO_4$ has a suitable saturation capacity for $Cs^+$ (113.47 mg/g) and $Sr^{2+}$ (109.11 mg/g). The batch experiments found that the optimum adsorption equilibrium time was about 60 min at 298 K and pH = 7 for all studied metal ions. The experimental results show the high thermal stability of the sorbent material until 500 °C. Finally, $MoTiWPO_4$ is a proficient sorbent material for removing both $^{137}$Cs and $^{85}$Sr from low-level-liquid radioactive waste samples by % eff. of 92.5 and 90.3, respectively, with high DF values.

**Author contribution** Abeer Kassem: experimental work, reviewing, and editing. Ezzat Abdel Galil: experimental work and editing. Sara S. Mahrous: data curation, preparing sorbent, writing — original draft review and editing.

**Funding** Open access funding provided by The Science, Technology & Innovation Funding Authority (STDF) in cooperation with The Egyptian Knowledge Bank (EKB).

**Data availability** Yes.

## Declarations

**Ethical approval** Yes.

**Consent to participate** Yes.

**Consent for publication** Yes.

**Competing interests** The authors declare no competing interests.



## References

Abass MR, El-Kenany WM, EL-Masry EH (2022) High efficient removal of lead(II) and cadmium(II) ions from multi-component aqueous solutions using polyacrylic acid acrylonitrile talc nanocomposite. Environ Sci Pollut Res 29:72929–72945. https://doi.org/10.1007/s11356-022-21023-1

Abdel-Galil EA, Moloukhia H, Abdel-Khalik M, Mahrous SS (2018) Synthesis and physico-chemical characterization of cellulose/HO7Sb3 nanocomposite as adsorbent for the removal of some radionuclides from aqueous solutions. Appl Radiat Isot 140:363–373. https://doi.org/10.1016/j.apradiso.2018.07.022

Abdel-Galil EA, Hassan RS, Eid MA (2019) Assessment of nano-sized stannic silicomolybdate for the removal of 137 Cs, 90 Sr, and 141 Ce radionuclides from radioactive waste solutions. Appl Radiat Isot 148:91–101. https://doi.org/10.1016/j.apradiso.2019.03.029

Abdel-Galil EA, Tourky AS, Kasem AE (2020) Sorption of some radionuclides from nuclear waste effluents by polyaniline/SiO2 composite: characterization, thermal stability, and gamma irradiation studies. Appl Radiat Isot 156:109009. https://doi.org/10.1016/j.apradiso.2019.109009

Abdel-Galil EA, Ibrahim AB, El-Kenany WM (2021) Facile fabrication of a novel silico vanadate ion exchanger: evaluation of its sorption behavior towards europium and terbium ions. Desalin Water Treat 226:303–318. https://doi.org/10.5004/dwt.2021.27261

Akinhanmi TF, Ofudje EA, Adeogun AI et al (2020) Orange peel as low-cost adsorbent in the elimination of Cd(II) ion: kinetics, isotherm, thermodynamic and optimization evaluations. Bioresour Bioprocess 7:34. https://doi.org/10.1186/s40643-020-00320-y

Ali MMS, Abdel-Galil EA, Hamed MM (2020) Removal of strontium radionuclides from liquid scintillation waste and environmental water samples. Appl Radiat Isot 166:109357. https://doi.org/10.1016/j.apradiso.2020.109357

Amesh P, Suneesh AS,Venkatesan KA et al (2020) Preparation and ion exchange studies of cesium and strontium on sodium iron titanate. Sep Purif Technol 238:116393

Attallah MF, Allan KF, Mahmoud MR (2016) Synthesis of poly(acrylic acid–maleic acid)SiO2/Al2O3 as novel composite material for cesium removal from acidic solutions. J Radioanal Nucl Chem 307:1231–1241. https://doi.org/10.1007/s10967-015-4349-1

Bediako JK, Lin S, Sarkar AK et al (2020) Evaluation of orange peel-derived activated carbons for treatment of dye-contaminated wastewater tailings. Environ Sci Pollut Res 27:1053–1068. https://doi.org/10.1007/s11356-019-07031-8

Cheng J, Liu K, Li X et al (2020) Nickel-metal-organic framework nanobelt based composite membranes for efficient Sr2+ removal from aqueous solution. Environ Sci Ecotechnology 3:100035. https://doi.org/10.1016/j.ese.2020.100035

El Afifi EM, Mansy MS, Hilal MA (2023) Radiochemical signature of radium-isotopes and some radiological hazard parameters in TENORM waste associated with petroleum production: a review study. J Environ Radioact 256:107042. https://doi.org/10.1016/j.jenvrad.2022.107042

El-Aryan YF, El-Said H, Abdel-Galil EA (2014) Synthesis and characterization of polyaniline-titanium tungstophosphate; its analytical applications for sorption of Cs+, Co2+, and Eu3+from waste solutions1. Radiochemistry 56:614–621. https://doi.org/10.1134/S106636221406006X

El-Din AMS, Monir T, Sayed MA (2019) Nano-sized Prussian blue immobilized costless agro-industrial waste for the removal of cesium-137 ions. Environ Sci Pollut Res 26:25550–25563. https://doi.org/10.1007/s11356-019-05851-2

El-Naggar IM, Mowafy EA, Abdel-Galil EA et al (2010) Synthesis, characterization and ion-exchange properties of a novel organic-inorganic hybrid cation-exchanger: polyacrylamide Sn(IV) molybdophosphate. Global J Phys Chem 1:91–106

El-Nagaar IM, Mahmoud MY, Abdel-Galil E (2012) Inorganic ion exchange materials based on titanate : synthesis, characterization and sorption behaviour of zirconium titanate for some hazardous metal ions from. Isot RAD RES 44:851–871

El-Naggar IM, Hebash KA, Sheneshen ES et al (2014) Preparation, characterization and ionexchange properties of a new organic-inorganic composite cation exchanger polyaniline silicotitanate: Its applications for treatment of hazardousmetal ions from waste solutions. Inorg Chem 9:1–14

Feng B, Onda Y, Wakiyama Y et al (2022) Persistent impact of Fukushima decontamination on soil erosion and suspended sediment. Nat Sustain 5:879–889. https://doi.org/10.1038/s41893-022-00924-6

Hassan RS, Eid MA, El-Sadek AA, Mansy MS (2019) Preparation, characterization and application of Mg/Fe Hydrotalcite as gamma sealed source for spectroscopic measurements. Appl Radiat Isot 151:74–80. https://doi.org/10.1016/j.apradiso.2019.04.040

Hilal MA, Attallah MF, Mansy MS, El Afifi EM (2022) Examination of the parameters affecting of 222Rn emanation for some industrial and environmental samples using gamma-spectroscopy. Appl Radiat Isot 186:110272. https://doi.org/10.1016/j.apradiso.2022.110272

Lagergreen S (1907) Zur Theorie der sogenannten Adsorption gelöster Stoffe. Zeitschrift Für Chemie Und Ind Der Kolloide 2:15. https://doi.org/10.1007/BF01501332

Le Hai T, Hung LC, Phuong TTB et al (2020) Multiwall carbon nanotube modified by antimony oxide (Sb2O3/MWCNTs) paste electrode for the simultaneous electrochemical detection of cadmium and lead ions. Microchem J 153:104456. https://doi.org/10.1016/j.microc.2019.104456

Lee HK, Jun BM, Kim S Il et al (2022) Simultaneous removal of suspended fine soil particles, strontium and cesium from soil washing effluent using inorganic flocculants. Environ Technol Innov 27. https://doi.org/10.1016/j.eti.2022.102467

Li H, Dong X, da Silva EB et al (2017) Mechanisms of metal sorption by biochars: biochar characteristics and modifications. Chemosphere 178:466–478. https://doi.org/10.1016/j.chemosphere.2017.03.072

Mahrous SS, Abdel-Galil EA, Belacy N, Saad EA (2019) Adsorption behavior and practical separation of some radionuclides using cellulose/HO7Sb3. Desalin Water Treat 152:124–132. https://doi.org/10.5004/dwt.2019.23981

Mahrous SS, Abass MR, Mansy MS (2022a) Bentonite phosphate modified with nickel: preparation, characterization, and application in the removal of 137Cs and 152+154Eu. Appl Radiat Isot 190:110445. https://doi.org/10.1016/j.apradiso.2022.110445

Mahrous SS, Galil EAA, Mansy MS (2022b) Investigation of modified orange peel in the removal of Cd2+, Co2+ and Zn2+ from wastewater. J Radioanal Nucl Chem 331:985–997. https://doi.org/10.1007/s10967-021-08166-0

Mahrous SS, Mansy MS, Abdel Galil EA (2022c) Decontamination of 137Cs,95Zr, 154Eu and 144Ce from aqueous solutions using polyacrylamide titanium tungstosilicate. J Radioanal Nucl Chem 331:4731–4744. https://doi.org/10.1007/s10967-022-08583-9

Mansy MS, Hassan RS, Selim YT, Kenawy SH (2017) Evaluation of synthetic aluminum silicate modified by magnesia for the removal of 137Cs, 60Co and 152+154Eu from low-level radioactive waste. Appl Radiat Isot 130:198–205. https://doi.org/10.1016/j.apradiso.2017.09.042

Mansy MS, Eid MA, Breky MME, Abass MR (2023) Sorption behavior of 137Cs, 152+154Eu and 131Ba from aqueous solutions using inorganic sorbent loaded on talc. J Radioanal Nucl Chem. https://doi.org/10.1007/s10967-023-08977-3

Nasseh N, Nasseh I, Khodadadi M et al (2017) The removal of lead from aqueous solution using almond green hull (Prunus amygdalus-Fascionello) waste material magnetized with Fe3O4. Ann Mil Heal Sci Res 15:1–7. https://doi.org/10.5812/amh.66336

Olabemiwo FA, Tawabini BS, Patel F et al (2017) Cadmium removal from contaminated water using polyelectrolyte-coated industrial waste fly ash. Bioinorg Chem Appl 2017:7298351. https://doi.org/10.1155/2017/7298351

Pandiarajan A, Kamaraj R, Vasudevan S, Vasudevan S (2018) OPAC (orange peel activated carbon) derived from waste orange peel for the adsorption of chlorophenoxyacetic acid herbicides from water: adsorption isotherm, kinetic modelling and thermodynamic studies. Bioresour Technol 261:329–341. https://doi.org/10.1016/j.biortech.2018.04.005

Patra K, Sengupta A, Mishra RK et al (2022) Assessing the feasibility study of highly efficient and selective co-sequestration process for cesium and strontium utilizing calix-crown and crown-ether based combined solvent systems. J Radioanal Nucl Chem 331:1473–1481. https://doi.org/10.1007/s10967-022-08209-0

Pham TT, Ngo HH, Tran VS, Nguyen MK (2020) Removal of As (V) from the aqueous solution by a modified granular ferric hydroxide adsorbent. Sci Total Environ 706:135947. https://doi.org/10.1016/j.scitotenv.2019.135947

Rizk SE, Hamed MM (2015) Batch sorption of iron complex dye, naphthol green B, from wastewater on charcoal, kaolinite, and tafla. Desalin Water Treat 56:1536–1546. https://doi.org/10.1080/19443994.2014.954004

Șenilă M, Neag E, Tănăselia C, Șenilă L (2023) Removal of cesium and strontium ions from aqueous solutions by thermally treated natural zeolite. Materials (Basel) 16

Solińska A, Bajda T (2022) Modified zeolite as a sorbent for removal of contaminants from wet flue gas desulphurization wastewater. Chemosphere 286:131772. https://doi.org/10.1016/j.chemosphere.2021.131772

Sopapan P, Lamdab U, Akharawutchayanon T et al (2023) Effective removal of non-radioactive and radioactive cesium from wastewater generated by washing treatment of contaminated steel ash. Nucl Eng Technol 55:516–522. https://doi.org/10.1016/j.net.2022.10.007

Stäger F, Zok D, Schiller AK, Feng B, Steinhauser G (2023) Disproportionately high contributions of 60 year old weapons-137Cs explain the persistence of radioactive contamination in bavarian wild boars. Environ Sci Technol 57(36):13601–13611. https://doi.org/10.1021/acs.est.3c03565

Tourky A, Abdel-Galil E, Kasem A et al (2016) Synthesis and Application of Polyacrylamide Sn(IV) Silicovanadate for Sorption of Some Radionuclides. J Nucl Technol Appl Sci 4:35–50

Vasiliev AN, Ermolaev SV, Lapshina EV et al (2019) 225Ac/213Bi generator based on inorganic sorbents. Radiochim Acta 107:1203–1211. https://doi.org/10.1515/ract-2019-3137

Yang HM, Park CW, Kim I et al (2021) Sulfur-modified chabazite as a low-cost ion exchanger for the highly selective and simultaneous removal of cesium and strontium. Appl Surf Sci 536:147776. https://doi.org/10.1016/j.apsusc.2020.147776

Yao C, Dai Y, Chang S, Zhang H (2022) Removal of cesium and strontium for radioactive wastewater by Prussian blue nanorods. Environ Sci Pollut Res. https://doi.org/10.1007/s11356-022-24618-w